

# Casimir forces between cylinders and plates

Sahand JamalRahi<sup>1</sup>, Thorsten Emig<sup>2,3</sup>, Robert L. Jaeger<sup>1,4</sup> and Mehran Kardar<sup>1</sup>

<sup>1</sup>Massachusetts Institute of Technology, Department of Physics,  
77 Massachusetts Avenue, Cambridge, MA 02139, USA

<sup>2</sup>Institut für Theoretische Physik, Universität zu Köln, Zùlpicher Strasse 77, 50937 Köln, Germany

<sup>3</sup>Laboratoire de Physique Théorique et Modèles Statistiques,  
CNRS UMR 8626, Bât. 100, Université Paris-Sud, 91405 Orsay cedex, France

<sup>4</sup>Center for Theoretical Physics, Laboratory for Nuclear Science,  
Massachusetts Institute of Technology, Cambridge, MA 02139, USA

We study collective interaction effects that result from the change of free quantum electrodynamic field fluctuations by one- and two-dimensional perfect metal structures. The Casimir interactions in geometries containing plates and cylinders is explicitly computed using partial wave expansions of constrained path integrals. We generalize previously obtained results and provide a more detailed description of the technical aspects of the approach [1]. We find that the interactions involving cylinders have a weak logarithmic dependence on the cylinder radius, reflecting that one-dimensional perturbations are marginally relevant in 4D space-time. For geometries containing two cylinders and one or two plates, we confirm a previously found non-monotonic dependence of the interaction on the object's separations which does not follow from pair-wise summation of two-body forces. Qualitatively, this effect is explained in terms of fluctuating charges and currents and their mirror images.

## I. INTRODUCTION

Quantum effects like Casimir forces have become increasingly important as electronic and mechanical systems on the nanometer scale become more prevalent [2, 3]. Now mechanical oscillation modes of quasi one-dimensional structures such as nanowires or carbon nanotubes can be probed with high precision [4]. Generally, the behavior of such systems is influenced by the collective nature of fluctuation forces: The total interaction of a system of objects or particles cannot be obtained by simply adding the forces between all pairs. Instead one has to consider also 3-body and higher order interactions that become increasingly important with decreasing separations between the objects.

So far Casimir electrodynamic interactions have mostly been investigated for two objects: parallel plates [5], a rectilinear piston [6], plate-sphere interaction at asymptotically large distances [7] and for all separations only recently [8]. A previous letter summarized the results for a plate and a parallel cylinder [1]. While shape and geometry can strongly influence two-body Casimir interactions, it is also important to understand the consequences of the non-additivity of fluctuation forces. In addition, the extent to which fluctuations are correlated depends on the effective dimensionality of the space that can be explored by the fluctuations. Therefore, Casimir interactions are expected to depend strongly on the codimension of the interacting objects [9].

In this work we concentrate on two central aspects of fluctuation forces: Effects resulting from the non-additivity and the particular properties of systems with

a codimension of the critical value of two. We consider these problems in the context of interactions between cylinders and sidewalls. In previous works we have demonstrated that Casimir forces in these geometries have only a weak logarithmic dependence on the cylinder radius [1] and can be non-monotonic [10, 11] { consequences of codimension and non-additivity. Here we employ and extend previously developed methods [1] to obtain the exact interaction between two perfect metal cylinders and its modification due to sidewalls from a partial wave expansion. These geometries are of recent experimental interest since cylinders are easier to hold parallel and generate a force that is extensive in its length [12].

In analogy to the cylinder-plate interaction [1], we obtain a weak logarithmic dependence on the cylinder radii  $R$  for the interaction  $E \sim cL = \frac{1}{2} \log(d=R_1) \log(d=R_2)$  between two parallel cylinders at asymptotically large distance  $d \gg R$ . We include higher order partial waves to describe the crossover between the asymptotic expression and the interaction at very short separations where the proximity force approximation (PFA) gives the correct zeroth order approximation to the Casimir energy. For two cylinders of equal radius  $R$ , it has the form  $E_{\text{PFA}}^{\text{cyl-cyl}} = \frac{3}{1920} \sim cL \frac{R}{(d-2R)^2}$  [11]. When one or two perfectly conducting sidewalls are added to a pair of cylinders, the force between the cylinders depends non-monotonically on the sidewall separation  $H$  [11]. We compute the interaction between the cylinders and the cylinder and the sidewall over a wide range of separations by employing the method of images and by summing numerically a large number of partial wave contributions. The non-monotonic behavior is found to result from a competition between force contributions from transverse magnetic (TM) and electric (TE) modes

Electronic address: kardar@mit.edu

which induce opposite image sources. The TE and TM forces between two cylinders are monotonically increasing and decreasing with the separation of the plate, respectively; their sum behaves non-monotonic because the slopes are different.

The rest of the paper is organized as follows. In the following Section we describe the methodology of our path integral approach and derive the elements of the relevant matrix operators for cylinders and sidewalls in a partial wave basis. In Section III we obtain analytical and numerical results for the forces between cylinders and sidewalls. Experimental implications and corrections for cylinders of finite length are discussed in Section IV. More technical steps of the calculations are relegated to the Appendices.

## II. METHODS

### A. Path integral and partial waves

We consider geometries that are composed of infinitely long cylinders and infinitely extended plates that are oriented such that the cylinder axes are all parallel and coincide with an in-plane axis of the plates that are also parallel to each other. Hence, the geometries have one continuous translational symmetry. This allows the electromagnetic modes to be split into transversal magnetic (TM) modes, described by a scalar field with Dirichlet (D) boundary conditions, and transversal electric (TE) modes, described by a scalar field obeying Neumann (N) boundary conditions. After a Wick rotation to the imaginary frequency ( $q_0$ ) axis, the action for the scalar field has the simple form

$$S = \frac{1}{2} \int_0^Z dq_0 \int d^3x (\dot{x}^2 + q_0^2 x^2) : \quad (1)$$

For the implementation of the boundary conditions and the computation of the interaction energy, we employ the techniques derived in references [1, 13, 14, 15]. After introducing an auxiliary field on each boundary to enforce the boundary conditions and integrating out the scalar field, one obtains an effective quadratic action for the auxiliary fields with kernel

$$M(u; u^0; q_0) = G_0(s(u); s(u^0); q_0) \quad (2)$$

for D conditions and

$$M(u; u^0; q_0) = \mathcal{G}_n(u) \mathcal{G}_n(u^0) G_0(s(u); s(u^0); q_0) \quad (3)$$

for N conditions, where the indices  $i, j$  label the surfaces. Here  $G_0(x; x^0; q_0) = e^{iq_0 x - q_0^0 x^0} = 4 \int \frac{d^3k}{(2\pi)^3} e^{i\mathbf{k} \cdot \mathbf{x} - i k^0 x^0}$  is the free space Green's Function and  $s(u)$  is a vector pointing to the  $i$ th surface parametrized by the coordinate vector  $u$  which describes a surface in 3D, so that it stands for two independent parameters, e.g., for a cylinder  $u = (x_1; \theta)$  with  $x_1$  oriented parallel the cylinder axis and  $\theta$  the azimuthal angle. When we integrate over the auxiliary fields, we finally obtain the Casimir energy for D and N modes at zero temperature [15],

$$E^{D=N} = \frac{\sim C}{2} \int_0^Z dq_0 \text{Tr} \log(M M^{-1}) : \quad (4)$$

The total electromagnetic Casimir energy is the sum of the energies  $E^D$  and  $E^N$ . The force between two objects separated by  $a$  can be computed by differentiating the energy,

$$F^{D=N} = - \frac{\sim C}{2} \int_0^Z dq_0 \text{Tr} M^{-1} r_a M : \quad (5)$$

The trace runs over the coordinates  $u$  and the indices  $i, j$ .  $M^{-1}$  is the functional inverse of  $M$  with all surfaces infinitely separated from one another.

Since the surfaces are static and since the system is invariant under translations along the  $u_1$ -direction of the cylinder axes, it is useful to transform the kernel  $M$  to momentum space where it is diagonal with respect to the momenta  $q_0$  and  $q_1$ . If we denote by  $\tilde{M}(q_0; q_1)$  the Fourier transformed matrix that is non-diagonal with respect to the remaining momenta  $q_2, q_2^0$ , the energy can be expressed in terms of the determinant of that matrix,

$$\begin{aligned} E^{D=N} &= \frac{\sim cL}{8} \int_0^Z dq_0 dq_1 \log k \tilde{M}(q_0; q_1) \tilde{M}^{-1}(q_0; q_1) k \\ &= \frac{\sim cL}{4} \int_0^Z dq_0 \log k \tilde{M}(q) \tilde{M}^{-1}(q) k \end{aligned} \quad (6)$$

with  $q = \sqrt{q_0^2 + q_1^2}$  and  $L$  the overall extent of the system along the  $u_1$ -axis. Hence  $\tilde{M}$  is a block-diagonal matrix of finite size. The blocks are indexed by  $i, j$  and the momenta  $q_2, q_2^0$  which may take discrete or continuous values depending on whether the corresponding surface is compact (cylinder) or infinitely extended (plate) along the  $u_2$ -direction. The matrix elements are defined by the Fourier integrals

$$M_{ij}(q) \tilde{M}^{-1}_{ji}(q) = \int_0^Z G(s^i(u_2) | s^j(u_2^0); q) e^{-iq_2 u_2 + iq_2^0 u_2^0} \frac{du_2 du_2^0}{2} \quad (7)$$

for D modes and

$$\text{Im } \mathcal{M}_{22}^{-1}(q) \mathcal{J}_2^0 = \int_{\mathbb{Z}} \mathcal{G}_n(u_2) \mathcal{G}_n(u_2^0) G(s^2(u_2) \cdot s^2(u_2^0); q) e^{-iq_2 u_2 + iq_2^0 u_2^0} \frac{du_2 du_2^0}{2} \quad (8)$$

for N modes where  $G(x^2; q)$  is the  $x_1$  Fourier transformed free Green's function and  $s^2(u_2)$  is the projection of  $s(u_2)$  onto the  $x_2$ - $x_3$ -plane that is perpendicular to the direction of translational invariance.

After obtaining the matrix elements the determinant of  $\mathcal{M} \mathcal{M}^{-1}$  needs to be computed. For  $n$  objects  $\mathcal{M}$  and  $\mathcal{M}^{-1}$  obviously have  $n \times n$  blocks each of which is indexed by  $q_2, q_2^0$ . For two objects we make use of the block matrix determinant formula

$$\begin{aligned} \begin{vmatrix} \mathcal{M}_{11} & \mathcal{M}_{12} \\ \mathcal{M}_{21} & \mathcal{M}_{22} \end{vmatrix} &= k \mathcal{M}_{11} k \mathcal{M}_{22} - \mathcal{M}_{21} \mathcal{M}_{11}^{-1} \mathcal{M}_{12} k \\ &= k \mathcal{M}_{22} k \mathcal{M}_{11} - \mathcal{M}_{12} \mathcal{M}_{22}^{-1} \mathcal{M}_{21} k : (9) \end{aligned}$$

For more than two objects one could recursively reduce the size of the matrix to compute its determinant. If the objects are infinite plates, a simpler approach is to employ the method of images which amounts to replace the free space Green's function by the Green's function for half-spaces or slabs.

## B. Two cylinders

We begin by considering two cylinders at center-to-center distance  $d$  of the general geometry shown in Fig. 1. The positions of the surfaces are parametrized in the  $x_2$ - $x_3$ -plane by

$$s_2^2(u) = (R_1 \sin u; R_1 \cos u) \quad (10)$$

$$s_3^2(u) = (R_2 \sin u + d; R_2 \cos u); \quad (11)$$

where the parametrization coordinate here is  $u_2 = u$ . With this parametrization, the matrix elements defined in Eqs. (7), (8) can be computed straightforwardly. We end (for details see Appendix A)

$$\text{Im } \mathcal{M}_{22}^{-1} \mathcal{J}_2^0 = \int_{\mathbb{Z}} \mathcal{G}_m(u) \mathcal{G}_m(u^0) I_m(R_1 q) K_m(R_1 q) \quad (12)$$

$$\text{Im } \mathcal{M}_{23}^{-1} \mathcal{J}_2^0 = \int_{\mathbb{Z}} \mathcal{G}_m(u) \mathcal{G}_m(u^0) I_m(R_1 q) I_m^0(R_2 q) K_m(u - u^0; qd) : \quad (13)$$

for D boundary conditions. The matrix elements of  $\mathcal{M}_{23}$  for N boundary conditions are obtained through differentiation of the matrix elements of  $\mathcal{M}_{23}$  for D boundary conditions with respect to  $R_1$  and  $R_2$ . The elements of the diagonal blocks for N boundary conditions are given by

$$\text{Im } \mathcal{M}_{22}^{-1} \mathcal{J}_2^0 = \int_{\mathbb{Z}} \mathcal{G}_m(u) \mathcal{G}_m(u^0) I_m^0(R_1 q) K_m^0(R_1 q) : \quad (14)$$

The matrix elements of  $\mathcal{M}_{33}$  are given by Eqs. (12) and (14) with  $R_1$  replaced by  $R_2$  and  $\mathcal{M}_{32} = \mathcal{M}_{23}^T$ . Using

the determinant formula of Eq. (9) and the fact that the off-diagonal matrix elements vanish for  $d \neq 0$ , we get

$$k \mathcal{M}_{11}^{-1} k = k I - \mathcal{M}_{32} \mathcal{M}_{22}^{-1} \mathcal{M}_{23} \mathcal{M}_{33}^{-1} k : \quad (15)$$

Hence, the interaction energy of the two cylinders can be obtained from Eq. (6) and the matrix elements

$$\begin{aligned} \text{Im } \mathcal{M}_{32} \mathcal{M}_{22}^{-1} \mathcal{M}_{23} \mathcal{M}_{33}^{-1} \mathcal{J}_2^0 &= \sum_n \mathcal{Z}_{m,n}^X(1; 1) K_{m+n}(qd) \mathcal{Z}_{n,n}^X(2; 2) K_{n+m}(qd); \quad (16) \end{aligned}$$

with  $X = D, N$  standing for Dirichlet and Neumann boundary conditions and the definitions

$$\mathcal{Z}_{m,n}^D(i; j) = \frac{I_m(R_i q)}{K_m(R_j q)} \quad (17)$$

$$\mathcal{Z}_{m,n}^N(i; j) = \frac{I_m^0(R_i q)}{K_m^0(R_j q)} : \quad (18)$$

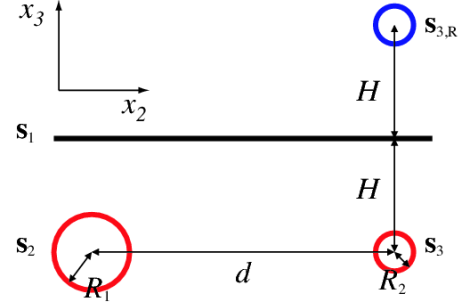


FIG. 1: Surfaces and parameters used for computing matrix elements. Surface  $S_3$  is displaced by  $d$  to the right of surface  $S_2$ . Surface  $S_3$  reflected at the plate yields surface  $S_{3R}$ .

## C. Cylinders and plates: Method of images

Now we add infinite plates to the geometry, see Fig. 1. The effective number of surfaces can be kept the same when adding the plates to the system if instead of the free space Green's function,  $G_0$ , modified Green's functions are used, which obey Dirichlet or Neumann boundary conditions at the plates. For one plate the half-space Green's function is

$$G_{1p}^X(x; x^0; q_0) = G_0(x; x^0; q_0) \pm s^X G_0(x; x_R^0; q_0) \quad (19)$$

where  $x_R^0 = (x_1; x_2; x_3 + 2H)$  is the reflection of  $x^0$  at the plane at  $x_3 = H$  and  $s^D = +1$ ,  $s^N = -1$ . For

two plates infinitely many images have to be used since successive reflections at the plates generate a series of images with increasing separation from the plates. For this slab geometry, the Green's function can be written as the series

$$\begin{aligned} G_{2p}^x(x; x^0; q_0) = & G_0(x; x^0; q_0) \\ & + \sum_{n=1}^{\infty} [G_0(x; x_{R1}^0; q_0) + G_0(x; x_{R2}^0; q_0)] \\ & + \sum_{n=1}^{\infty} [G_0(x; x_{R1R2}^0; q_0) + G_0(x; x_{R2R1}^0; q_0)] \\ & + \dots \end{aligned} \quad (20)$$

where  $x_{R1}^0, x_{R2}^0, \dots$  is obtained from  $x^0$  by a sequence of reflections at plate 1, 2, ... The theory developed for the free space at the beginning of this Section applies also to half-space and slab geometry. The interaction between a set of cylinders in the presence of one or two parallel plates can be obtained again from Eq. (6); one only needs to substitute the half-space or slab Green's functions for  $G$  in Eqs. (7), (8) and then obtain cylinder-cylinder matrix elements. When using these image Green's functions, their appropriate Fourier transformed matrices shall be labeled  $M_{1p}^*$  and  $M_{2p}^*$ .

Below, we shall consider the two cylinders  $S_2$  and  $S_3$ , see Fig. 1. The surfaces of the reflected cylinders have the parametrization

$$s_{2,R}^2(\theta) = (R_1 \sin \theta; R_1 \cos \theta + z) \quad (21)$$

$$s_{3,R}^2(\theta) = (R_2 \sin \theta + d; R_2 \cos \theta + z); \quad (22)$$

where  $z$  is a distance normal to the plates. Upon one reflection  $z$  is  $2H$  and the cylinder surface orientation is reversed, hence, the minus sign is chosen in Eqs. 21 and 22. For two plates the reflected cylinder is reflected again, so that the plus sign must be chosen for the orientation, and  $z = 2H_1 - 2H_2$  (if the first plate is located a distance  $H_1$  above and the second plate a distance  $H_2$  below the cylinder, see Fig. 6).

The corresponding matrix elements of Eqs. (7), (8) for D modes are

$$\begin{aligned} \text{Im } M_{2(2,R)}^{(0)} i = & (-1)^{m_0} I_m(R_1 q) I_{m_0}(R_1 q) K_{m-m_0}(q) : \\ \text{Im } M_{2(3,R)}^{(0)} i = & (-1)^{m_0} \frac{i d}{2 + d^2} \frac{I_m(R_1 q) I_{m_0}(R_2 q) K_{m-m_0}(q)}{p^2 + d^2} : \end{aligned} \quad (23)$$

The elements of  $M_{3(3,R)}^*$  follow from those of  $M_{2(2,R)}^*$  by replacing  $R_1$  by  $R_2$  and the elements of  $M_{3(2,R)}^*$  are given by those of  $M_{2(3,R)}^*$  with  $R_1$  and  $R_2$  interchanged and  $d$  replaced by  $-d$ . For N modes, the elements of  $M_{2(2,R)}^*$  are obtained by differentiation of the D elements with respect to  $R_1$  and  $R_2$ . The elements of  $M_{2(2,R)}^*$  for N modes are given by

$$\text{Im } M_{2(2,R)}^{(0)} i = (-1)^{m_0} q^2 I_m^0(R_1 q) I_{m_0}^0(R_1 q) K_{m-m_0}(q) : \quad (24)$$

### III. INTERACTION ENERGIES

#### A. Two cylinders

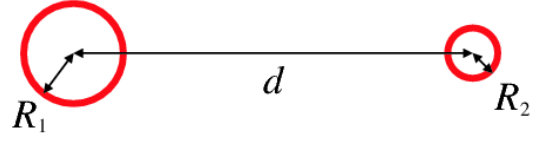


FIG. 2: Cylinder-cylinder geometry.

We consider two cylinders of radii  $R_1$  and  $R_2$  with center-to-center separation  $d$ , see Fig. 2. For this geometry the interaction energy is obtained from Eqs. (6) and (15) with the matrix elements of Eq. (16). For large separations  $d \gg R_1, R_2$ , the asymptotic behavior of the energy is determined by the matrix elements for  $m = m^0 = 0$  for D modes and  $m = m^0 = 0; \pm 1$  for N modes. Taking the determinant of the matrix that consists only of these matrix elements and integrating over  $q$  yields straightforwardly the attractive interaction energies

$$\begin{aligned} E^D = & \frac{\sim cL}{d^2} \frac{1}{8 \log(d=R_1) \log(d=R_2)} \\ & + \frac{1}{\log(d=R_1)} \frac{1}{\log(d=R_2)} + \dots; \quad (25) \\ E^N = & \sim cL \frac{7}{5} \frac{R_1^2 R_2^2}{d^6} : \end{aligned}$$

The asymptotic interaction is dominated by the contribution from TM (D) modes that vanishes for  $R \rightarrow 0$  only logarithmically.

For arbitrary separations higher order partial waves have to be considered. The number of partial waves has to be increased with decreasing separation. A numerical evaluation of the determinant and the  $q$ -integration can be performed easily and reveals an exponentially fast convergence of the energy in the truncation order for the partial waves. Down to small surface-to-surface separations of  $(d - 2R) = R = 0.1$  we find that  $m = 40$  partial waves are sufficient to obtain precise results for the energy. The corresponding result for the energies of two cylinders of equal radius is shown in Fig. 3. Notice that the minimum in the curve for the total electromagnetic energy results from the scaling by the PFA estimate of the energy. The total energy is monotonic and the force attractive at all separations.

#### B. Cylinder-plate geometry

The simplest geometry to which the method of images can be applied is composed of an infinite plate and a parallel cylinder of radius  $R$ , see Fig. 4. The Casimir energy for this geometry has been computed in Ref. [1] from the

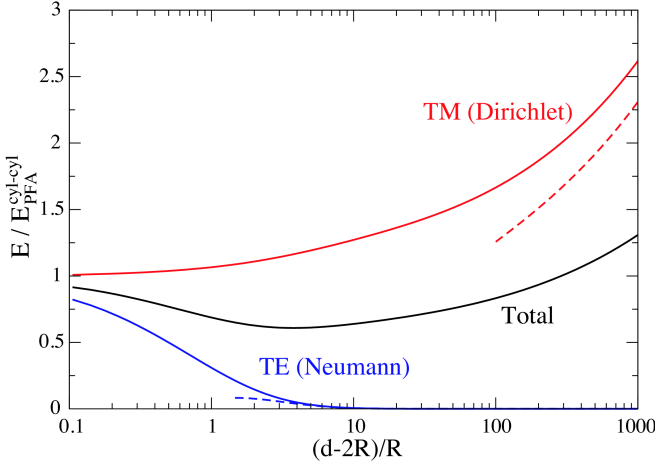


FIG. 3: Casimir energy for two cylinders of equal radius  $R$  as a function of surface-to-surface distance  $d - 2R$  (normalized by the radius). The energy is divided by the PFA estimate  $E_{\text{PFA}}^{\text{cyl-cyl}}$  for the energy given in the introduction. The solid curves show our numerical results; the dashed lines represent the asymptotic results of Eqs. 25. The  $l=\log$  corrections to the leading order result for TM modes cause very slow convergence.

matrix elements of Eqs. (7), (8) for the plate and the cylinder. Here, we employ the method of images so that we have to consider only one surface, the cylinder, that is placed into the half-space that is bounded by the plate. Hence, we substitute  $G$  by  $G_{1p}$  in Eq. (7), (8) together with the parametrizations of Eq. (11) and of Eq. (22) with the  $+$  sign,  $R_2 = R$  and  $z = 2H$ . The resulting  $\tilde{M}_{1p}$  is simply one block for the cylinder since there is effectively only one surface, and it equals  $\tilde{M}_{33} = \tilde{M}_{3(3R)}$ . When the plate is moved to infinite separation from the cylinder, there is only the free cylinder, so  $\tilde{M}_{1p;l}^{-1} = \tilde{M}_{33}^{-1}$ . The determinant of Eq. (6) can now be written as

$$\det \tilde{M}_{1p} \tilde{M}_{1p;l}^{-1} = \det \tilde{M}_{3(3R)} \tilde{M}_{33}^{-1} \quad (26)$$

The matrix elements of  $\tilde{M}_{3(3R)} \tilde{M}_{33}^{-1}$  are given for D modes by

$$\langle m | \tilde{M}_{3(3R)} \tilde{M}_{33}^{-1} | n \rangle = \frac{I_m(Rq)}{K_{m0}(Rq)} K_{m+m0}(2Hq) \quad (27)$$

and for N modes by

$$\langle m | \tilde{M}_{3(3R)} \tilde{M}_{33}^{-1} | n \rangle = \frac{I_m^0(Rq)}{K_{m0}^0(Rq)} K_{m+m0}(2Hq) \quad (28)$$

This result in combination with Eq. (6) is identical to the one given in Eqs. (5)–(8) of Ref. [1]. The asymptotic expression for the attractive interaction energy at  $H \gg R$  reads

$$\begin{aligned} E^D &= -\frac{cL}{H^2} \frac{1}{16 \log(H/R)}; \\ E^N &= -\frac{cL}{32} \frac{R^2}{H^4} \end{aligned} \quad (29)$$

The total electromagnetic Casimir interaction is again dominated by the contribution from the D mode with  $m = 0$  which depends only logarithmically on the cylinder radius. The interaction at all separations follows, as in the case of two cylinders, from a numerical computation of the determinant of Eq. (26) and integration over  $q$ . The result is shown in Fig. 5.

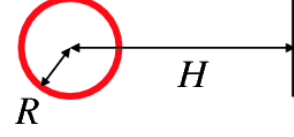


FIG. 4: Cylinder-plate geometry.

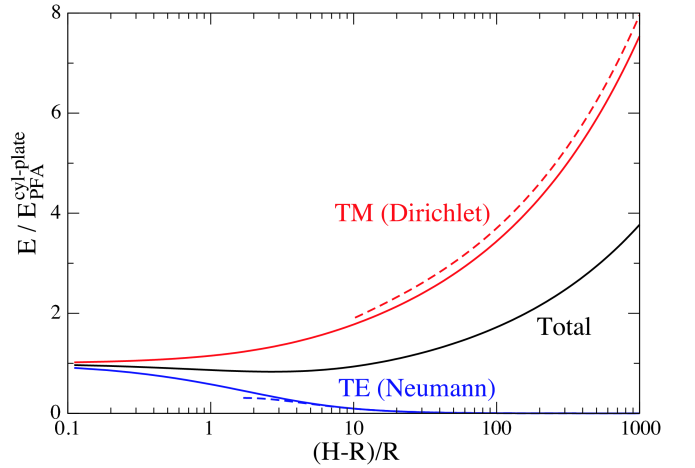


FIG. 5: Casimir energy for one cylinder of radius  $R$  parallel to one plate as a function of the surface-to-surface distance  $H - R$  (normalized by the radius). The energy is divided by the PFA estimate  $E_{\text{PFA}}^{\text{cyl-plate}}$  of energy given in the Introduction. The solid curves reflect our numerical results; the dashed lines represent the asymptotic results of Eqs. 29. Convergence for the TM (Dirichlet) energy to the asymptotic result is very slow because of  $l=\log$  corrections.

### C. Two cylinders, parallel to plate(s)

The image technique lends itself to studying multi-body interactions involving plates and cylinders. We consider the geometry shown in Fig. 6 with two cylinders that are placed parallel to one or in-between two parallel plates. Rodriguez et al. [10] studied a similar geometry consisting of two metal squares between two parallel metal sidewalls by computing numerically the mean stress tensor and observed that the force between the two squares changes non-monotonically when the two plates are pulled away. In previous work, we applied the stress tensor method and the path integral approach presented above to the geometry of Fig. 6 and found again a non-

monotonic dependence of the force between the cylinders on the separation between the plates [11]. Here we provide the technical details of the path integral approach and the method of images employed in the latter work.

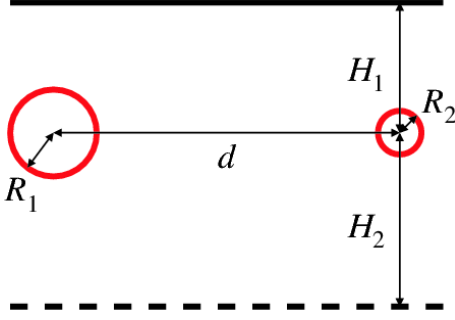


FIG. 6: Two cylinders parallel to one plate or sandwiched between two parallel plates.

To study the interaction between the cylinders and plates it turned out to be more convenient to compute directly the forces between the objects as defined by Eq. (5). For the force between the two cylinders we set  $\mathbf{a} = d\hat{x}_2$  and for the force between the cylinders and a plate we choose  $\mathbf{a} = H_1\hat{x}_3$ . The matrix  $\mathbf{M}$  of Eq. (5) can be constructed by the method of images as follows. We consider the two cylinders as the surfaces that are placed either inside a half-space or a slab so that the matrix elements of  $\mathbf{M}$  are given by Eqs. (7), (8) with  $G$  replaced by  $G_{1p}^x$  or  $G_{2p}^x$  of Eqs. (19), (20), respectively. We shall refer to the corresponding  $2 \times 2$  block matrices  $\tilde{\mathbf{M}}_{1p}$  and  $\tilde{\mathbf{M}}_{2p}$  matrices as  $\tilde{\mathbf{M}}_{np}$  which is of the form

$$\tilde{\mathbf{M}}_{np} = \begin{pmatrix} \tilde{\mathbf{M}}_{np;22} & \tilde{\mathbf{M}}_{np;23} \\ \tilde{\mathbf{M}}_{np;32} & \tilde{\mathbf{M}}_{np;33} \end{pmatrix} : \quad (30)$$

In the two-body cylinder case without sidewalls the  $\tilde{\mathbf{M}}$  matrix blocks describing the self-interaction were diagonal in  $m$ . Here, the self-interaction blocks  $\tilde{\mathbf{M}}_{np;}$  contain image information and are not diagonal. The matrix elements of  $\tilde{\mathbf{M}}_{np}$  are constructed from the elements of Eqs. (23), (24). Their explicit form and a formula for the inversion of  $\tilde{\mathbf{M}}_{np}$  are given in Appendix B. The integrand of Eq. (5) can be straightforwardly computed by truncating the matrix  $\mathbf{M}$  at a finite partial wave order  $m$  and performing the matrix multiplication and trace in Fourier space. Including up to  $m = 35$  partial waves, we obtain for the Casimir force between two cylinders of equal radii in the presence of one or two sidewalls the results shown in Fig. 7. In this figure the force at a fixed surface-to-surface distance  $d = 2R = 2R$  between the cylinders is plotted as a function of the relative separation  $(H - R)/R$  between the plate and cylinder surfaces. Two interesting features can be observed. First, the attractive total force varies non-monotonically with  $H$ : Decreasing for small  $H$  and then increasing towards the asymptotic limit between two isolated cylinders for large  $H$ , cf. Eq. (25). The extremum for the one-sidewall

case occurs at  $H - R = 0.27R$ , and for the two-sidewall case is at  $H - R = 0.46R$ . Second, the total force for the two-sidewall case in the proximity limit  $H = R$  is larger than for  $H = R + 1$ . As might be expected, the  $H$ -dependence for one sidewall is weaker than for two sidewalls, and the effects of the two sidewalls are not additive: not only is the difference from the  $H = 1$  force not doubled for two sidewalls compared to one, but the two curves actually intersect at a separation of  $H = R = 1.13$ .

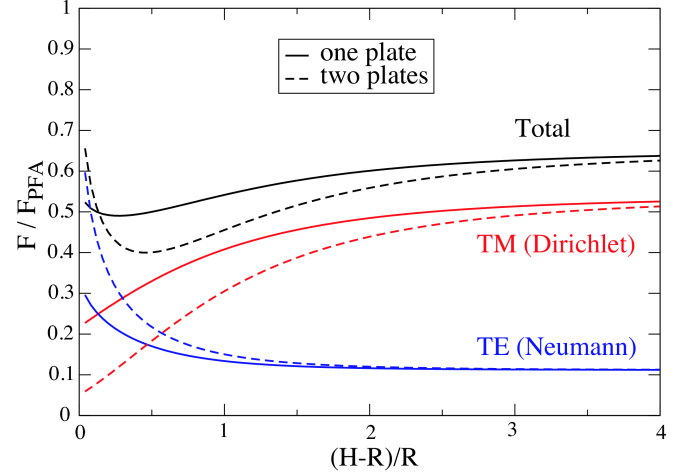


FIG. 7: Electromagnetic Casimir force per unit length between two cylinders for the geometry of Fig. 6 with  $H_1 = H_2 = H$  and  $R_1 = R_2 = R$  vs. the ratio of sidewall separation to cylinder radius  $(H - R)/R$ , at fixed distance  $(d - 2R)/R = 2$  between the cylinders, normalized by the total PFA force per unit length between two isolated cylinders  $F_{PFA} = \frac{5}{2} (\sim c^3/1920) \sqrt{R} = (d - 2R)^{7/2}$  [11]. The force is attractive. The solid lines refer to the case with one sidewall, while dashed lines depict the results for two sidewalls. Also shown are the individual TE (blue) and TM (red) forces.

A simple generic argument for the non-monotonic sidewall effect has been given in Ref. 11. It arises from a competition between the force from TE and TM modes as demonstrated by the results in Fig. 7. An intuitive perspective for the qualitatively different behavior of the TE and TM force as a function of the sidewall distance is obtained from the method of images. For the D modes (TM polarization) the Green's function of Eq. (19) is obtained by subtracting the contribution from the image so that the image sources have opposite signs. Any configuration of fluctuating TM charges on one cylinder is thus screened by images, more so as  $H$  is decreased, reducing the force on the fluctuating charges of the second cylinder. This is similar to the effect of a nearby grounded plate on the force between two opposite electrostatic charges. Since the reduction in force is present for every charge configuration, it is there also for the average over all configurations, accounting for the variations of the TM curves in Fig. 7.

By contrast, the N modes (TE polarization) require image sources of the same sign as demonstrated by the

half-space Green's function of Eq. (19). The total force between actuating sources on the cylinders is now larger and increases as the plate separation  $H$  is reduced. (An analogous additive effect occurs for the classical force between current loops near a conducting plane.) Note, however, that while for each actuating source configuration, the effect of images is additive, this is not the case for the average over all configurations. More precisely, the effect of an image source on the Green's function is not additive because of feedback effects: the image currents change the surface current distribution, which changes the image, and so forth. For example, the net effect of the plate on the Casimir TE force is not to double the force as  $H \rightarrow R$ . The increase is in fact larger than two due to the correlated fluctuations.

In Fig. 8, we show the total force between the cylinders vs. the sidewall separation  $H=R$  for a variety of different values of the cylinder separation  $d=R$  in the presence of a single sidewall. As we vary  $d=R$  the depth of the minimum in the force changes, see Fig. 8. The separation  $(d-2R)/R = 2$  from Fig. 7 seems to achieve the largest value of non-monotonicity. For larger or smaller  $d$  the degree of non-monotonicity (defined as the difference between the minimum force and the force in the limit  $H \rightarrow 0$ ) decreases. For small  $d$ , the force approaches to PFA estimate. For large  $d$ , the TM (Dirichlet) force dominates except when the cylinders are sufficiently close to the metal plate when it is reduced enough by its image cylinder that the TE (Neumann) force takes over.

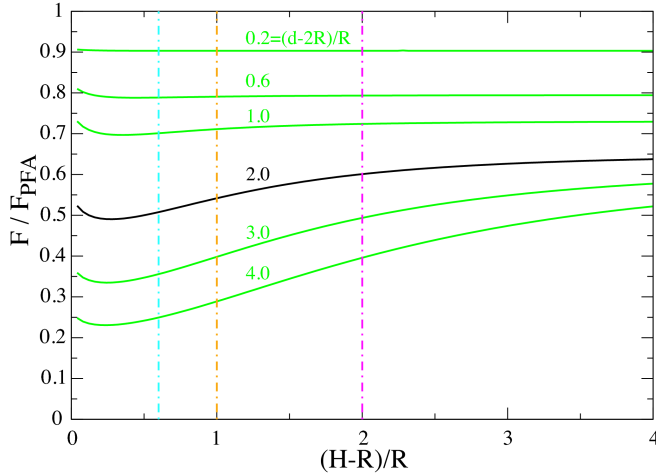


FIG. 8: Casimir force per unit length between two cylinders of equal radius vs. the ratio of sidewall separation to cylinder radius  $(H-R)/R$  (for one plate), normalized by the total PFA force per unit length between two isolated cylinders for various  $(d-2R)/R$ . The non-monotonic effect appears to become weaker as  $(d-2R)/R$  is moved away from 2. The vertical lines indicate the sidewall separations used in Fig. 9.

While the above arguments explain the competition between TE and TM forces, they do not show that the sum of these competing forces is non-monotonic. For example, if the TE and TM variations with  $H$  were equal

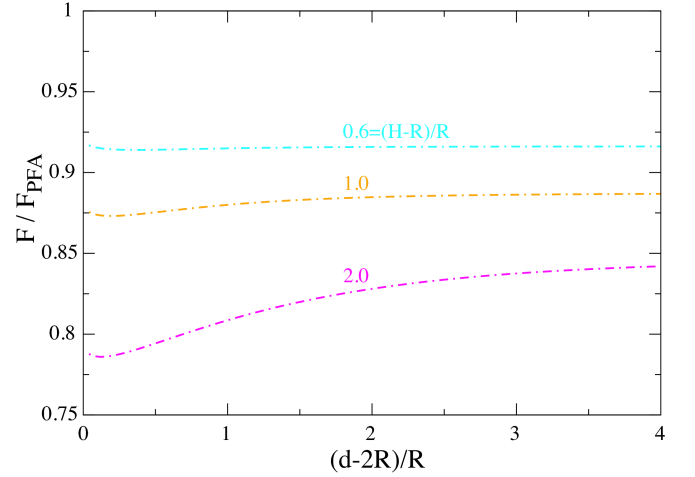


FIG. 9: Total Casimir force between two cylinders of equal radius  $R$  and a sidewall vs. the ratio of cylinder surface separation to cylinder radius  $(d-2R)/R$ , normalized by the total PFA force per unit length between a cylinder and a plate  $F_{\text{PFA}} = \frac{5}{2} (\sim c^3 = 960) \sqrt{R} = 2(d-2R)^{7/2}$  [16] for plate separations of  $H/R = 0.6R$ ,  $R$ , and  $2R$ . Note that the normalization is different from the cylinder-cylinder PFA in the previous figures.

and opposite, they would cancel with no net dependence on  $H$ . That this is not the case can be checked by examining the two limits  $H \rightarrow R$  and  $H \rightarrow R/R$ . In order to simplify the analysis, we assume that there is one sidewall and that in both limits the two cylinders have a large separation  $d \gg H/R, R$ . Then in the case  $H \rightarrow R/R$  the cylinders and their images are separated by a distance that is large compared to  $R$  so that the forces are dominated by the lowest partial waves, s-wave for TM and both s- and p-wave for TE modes [1]. The former is stronger and dominates the asymptotic force for which we obtain

$$\frac{F_D}{L} = \frac{4\pi c}{d^7 \ln^2(R=H)}; \quad (31)$$

confirming the reduced net force as the cylinders get closer to the plate.

It is instructive to justify the scaling of the force in Eq. (31) with  $H$  and  $d$  from simple physical arguments. While the logarithmic dependence on  $R$  could have been anticipated [1], the  $H^4$  scaling is a remarkable consequence of the multi-body effect. For TM modes, the field obeys Dirichlet boundary conditions so that the mirror source has opposite sign. Therefore, each cylinder and its mirror image can be considered as a dipole of size  $H$ . The interaction of the two dipoles should scale as the interaction between two cylinders of size  $H$  with Neumann boundary conditions. For  $d \gg H$  the force for the latter problem scales as  $H^4 = d^7$ , explaining the above result [1], up to the logarithm.

In the opposite limit  $H \rightarrow R/R$ , the image cylinder is very close to the original cylinder so that the interaction

involves partial waves of high order. In an attempt to analytically understand this limit, we performed certain asymptotic calculations reported in Appendix C. Since the relevance of the conclusions to the regime studied numerically (Fig. 7) is not clear, we shall not further explore the implications of these results. We note, however, that the numerical results in the regime of Fig. 7 support the dominance and fast decay of TE modes for this range of parameters, as justification for the non-monotonic behavior.

Thus far we have discussed the variation of the force between the two cylinders with the sidewall separation. We found that the force is not monotonic in  $H$ . This also implies that the force between the cylinders and the sidewalls is not monotonic in  $d$ . A non-monotonic force  $F_{x_2}$  between the cylinders means that there is a value of  $H$  where  $\partial F_{x_2}/\partial H = 0$ . Since the force is the derivative of the energy,  $F_{x_2} = -\partial E/\partial d$ , at this point  $\partial^2 E/\partial d \partial H = 0$ . These two derivatives, of course, can be interchanged to yield  $\partial(\partial E/\partial H)/\partial d = 0$ . But this means that  $\partial F_{x_3}/\partial d = 0$  at the same point, where  $F_{x_3} = -\partial E/\partial H$  is the force between the cylinders and the sidewall. This cylinders-sidewall force is plotted in Fig. 9 as a function of  $d/R$  for various values of  $H/R$  and clearly is non-monotonic in  $d/R$ . The non-monotonicity is smaller which is not surprising since the effect of a small cylinder on the force between two bodies is smaller than the effect of an infinite plate.

#### IV. DISCUSSION

In previous research, unusual Casimir force phenomena were sought by considering parallel plates with exotic materials: for example, repulsive forces were predicted using magnetic conductors [17], combinations of different dielectrics [18], fluids between the plates [19], and even negative-index media with gain [20]. A different approach is to use idealized materials such as perfect conductors with more complicated geometries: as illustrated in this and previous [10] work, surprising non-monotonic (attractive) effects can arise by considering as few as three objects. These effects arise from the collective properties of fluctuation forces and cannot emerge in a system of particles that interact by a pairwise two-body potential.

It would be interesting to probe the collective nature of fluctuation forces in experiments. So far, only the interaction between two objects, mostly for sphere-plate geometries, have been realized experimentally. Among the forces studied here, the one between two cylinders and a plate, see Fig. 9, might be most feasible in experimental studies. To measure the cylinder-plate force, the two cylinders need not be separated by vacuum—we expect that a similar phenomenon will arise if the cylinders are separated by a dielectric spacer layer of fixed thickness. This avoids the problem of parallelism one would face when measuring the force between two cylinders. Un-

fortunately, the non-monotonic effect in Fig. 9 is rather small (roughly 0.2%), but it may be possible to increase it by further optimization of the geometry and/or the material.

Another important issue is the translational invariance of the geometries considered here. The geometries of experimental tests will obviously lack this symmetry beyond some length scale. Hence it is important to study deviations from the here considered quasi-2D geometries due to cylinders and plates of finite size. Then the surfaces have to be treated as compact objects. For this full 3-dimensional problem, TM and TE modes are longer decoupled so that the full electromagnetic vector field has to be quantized. This can be done by a recently developed multipole expansion which yields the Casimir interaction between objects of arbitrary shape in terms of their T-matrices [21, 22]. At asymptotically large separations between the objects, the interaction is determined to leading order by the object's static electric and magnetic dipole polarizabilities. For a cylinder of finite length  $L \ll R$ , the component of the electric polarizability tensor along the cylinder axis scales as  $L^3 = \log(L/R)$ . Hence, the interaction energy between two parallel cylinders of finite length behaves for separations  $d \ll R$  as  $\sim c \log^2(L/R) d^{-7}$ . This result shows that for large  $d$  the interaction is no longer proportional to  $L$  or the product of the volume of the cylinders as might be expected in analogy with the Casimir-Polder interaction between spherical particles [1]. In fact, for large  $d$  the interaction amplitude scales as the product of the cubes of the largest dimensions of the objects. The cross-over between the two extreme cases of infinitely long cylinders and asymptotically large separations between finite-sized cylinders can be obtained in principle from a multipole expansion by including higher order multipoles. Finally, we note that all results given for infinitely long cylinders here can be also obtained within the T-matrix approach [21, 22]. The latter technique should be particularly useful to determine whether the same non-monotonic effects occur for two spheres next to a metal plate.

#### Acknowledgments

This work was supported in part by NSF grant DMR-04-26677 (SJR and MK), by the US Dept. of Energy (DOE) under cooperative research agreement DF-FC 02-94ER 40818 (RLJ), and by DFG grant EM 70/3 (TE).

#### APPENDIX A: MATRIX ELEMENTS

Here, we derive  $M_{22}$  and  $M_{23}$  based on Eqs. (7) and (8) for TM (Dirichlet) and TE (Neumann) modes in detail.

We compute  $M_{22}$  for Dirichlet boundary conditions as

follows:

$$\begin{aligned} \lim_{Z \rightarrow 0} \tilde{M}_{22}^{(0)} = & \int_0^{2\pi} \int_0^{2\pi} G(s_2^2(\phi) - s_2^2(\phi^0); q) e^{i(m\phi + m^0\phi^0)} \frac{d\phi d\phi^0}{2} = \\ & \int_0^{2\pi} \int_0^{2\pi} e^{ij(\phi - \phi^0)} I_j(qR_1) K_j(qR_2) e^{i(m\phi + m^0\phi^0)} \frac{d\phi d\phi^0}{(2\pi)^2} = \\ & \lim_{m \rightarrow 0} I_m(qR_1) K_m(qR_2); \end{aligned} \quad (A1)$$

The Green's function expansion in terms of modified Bessel functions of the first (I) and second kind (K) contains arguments  $r_<$  and  $r_>$ , for which the radius of  $s_2^2$  is inserted. Once the angular integrations are carried out one obtains in the last line the result of Eq. (12).

In order to compute  $\tilde{M}_{22}$  for Neumann boundary conditions with the least effort, we make use of the previous calculation. According to Eq. (8) the directional derivatives with respect to the surface normal of cylinders  $s_2^2(\phi)$  and  $s_2^2(\phi^0)$  need to be taken inside the integral. We simply assume that  $s_2^2(\phi)$  and  $s_2^2(\phi^0)$  are two different concentric cylinders with different radii  $R$  and  $R_1^0$ , respectively, and  $R_1 < R_1^0$  so that the derivatives  $\partial_{n_2(\phi)} \partial_{n_2(\phi^0)}$  are taken as  $\partial_{R_1} \partial_{R_1^0} I_j(qR_1) K_j(qR_1^0)$ . Then, the limit  $R_1^0 \rightarrow R_1$  is taken to yield Eq. (14).

The computation of  $\tilde{M}_{23}$  is more involved and is carried out without a convenient expansion of the Green's function. Eqs. (10) and (11) give the surface parametrizations which yield

$$\begin{aligned} \lim_{Z \rightarrow 0} \tilde{M}_{23}^{(0)} = & \int_0^{2\pi} \int_0^{2\pi} G(s_2^2(\phi) - s_2^2(\phi^0); q) e^{i(m\phi + m^0\phi^0)} \frac{d\phi d\phi^0}{2} = \\ & \int_0^{2\pi} \int_0^{2\pi} \frac{e^{ik(s_2^2(\phi) - s_2^2(\phi^0))} e^{i(m\phi + m^0\phi^0)}}{k^2 + q^2} \frac{d^2 k d\phi d\phi^0}{(2\pi)^3} = \\ & \int_0^{2\pi} \int_0^{2\pi} \frac{e^{i(k_1 R_1 \sin \phi + k_2 R_1 \cos \phi - k_1 (R_2 \sin \phi^0 + d) - k_2 R_2 \cos \phi^0)}}{k^2 + q^2} \frac{d^2 k d\phi d\phi^0}{(2\pi)^3} = \\ & \int_0^{2\pi} \int_0^{2\pi} \frac{e^{ik_1 d}}{k^2 + q^2} \frac{k_1 + ik_2}{k_1^2 + k_2^2} J_m(kR_1) \\ & \frac{k_1 + ik_2}{k_1^2 + k_2^2} J_m(qR_2) \frac{d^2 k}{2}; \end{aligned} \quad (A2)$$

where  $k = \sqrt{k_1^2 + k_2^2}$ . The limits of integration are, of course, 0 to  $2\pi$  for the angles  $\phi$  and  $\phi^0$  and 1 to 1 for the  $k_1$  and  $k_2$  integrals. Despite the appearance of square roots the above expression is analytical in the integration variables except for the simple poles due to  $k_1^2 + k_2^2 + q^2$  in the denominator. So, the  $k_1$  integration can be carried out by contour integration. If  $d$  is positive then the contour is closed in the lower half plane. The result

is Eq. (13):

$$\begin{aligned} \lim_{Z \rightarrow 0} \tilde{M}_{23}^{(0)} = & \int_0^{2\pi} \int_0^{2\pi} \frac{e^{i(m\phi + m^0\phi^0)} I_m(qR_1) I_m(qR_2)}{2} \frac{d\phi d\phi^0}{q^2 + k_2^2} e^{d \sqrt{q^2 + k_2^2}} \\ & \frac{\sqrt{q^2 + k_2^2}}{q} I_m(qR_1) I_m(qR_2) K_m(qd) = \\ & (i)^{m+m^0} I_m(qR_1) I_m(qR_2) K_m(qd); \end{aligned} \quad (A3)$$

$\tilde{M}_{23}$  for TE (Neumann) modes is easy to obtain. The derivatives in Eq. (8) can be taken out of the integral—they are just derivatives with respect to  $R_1$  and  $R_2$ —and applied to  $\tilde{M}_{23}$  for TM (Dirichlet) modes.

## APPENDIX B: INVERSE MATRIX AND MATRIX ELEMENTS FOR MULTIBODY FORCES

To compute forces according to Eq. (5) the matrix  $M$  or its Fourier transform  $\tilde{M}$  need to be inverted. For a  $2 \times 2$  block matrix the inverse can be written in terms of the inverses of the blocks,

$$\begin{pmatrix} A & B \\ C & D \end{pmatrix}^{-1} = \begin{pmatrix} (A - BD^{-1}C)^{-1} & A^{-1}B(D - CA^{-1}B)^{-1} \\ D^{-1}C(A - BD^{-1}C)^{-1} & (D - CA^{-1}B)^{-1} \end{pmatrix}; \quad (B1)$$

So, with  $\tilde{M}_{np} = [\tilde{M}_{np;22}, \tilde{M}_{np;23}, \tilde{M}_{np;32}, \tilde{M}_{np;33}]$  given,  $\tilde{M}_{np}^{-1}$  can be found, then the trace taken, to obtain the force.

To express  $\tilde{M}_{np}$  in terms of the matrix elements of  $\tilde{M}_{22}, \tilde{M}_{2(2;R)}, \tilde{M}_{23}$ , and  $\tilde{M}_{2(3;R)}$  we shall refer to their parameters in the following way

$$\begin{aligned} \tilde{M}_{2(2;R)} &= \tilde{M}_{2(2;R)}(\phi; \phi^0) \\ \tilde{M}_{23} &= \tilde{M}_{23}(d) \\ \tilde{M}_{2(3;R)} &= \tilde{M}_{2(3;R)}(d; \phi; \phi^0); \end{aligned} \quad (B2)$$

where the parameters refer to the notation in Eqs. (13), (23). The matrix blocks of  $\tilde{M}_{1p}$  are built up as follows:

$$\begin{aligned} \tilde{M}_{1p;22} &= \tilde{M}_{22} - s^x \tilde{M}_{2(2;R)}(2H; \phi) \\ \tilde{M}_{1p;23} &= \tilde{M}_{23}(d) - s^x \tilde{M}_{2(3;R)}(d; 2H; \phi); \end{aligned} \quad (B3)$$

Clearly,  $\tilde{M}_{1p;33}$  is obtained by replacing  $R_1$  by  $R_2$  and  $\tilde{M}_{1p;32} = \tilde{M}_{1p;23}^y$ . As before, one takes  $s^x = +1$  for Dirichlet and  $s^x = -1$  for Neumann modes. Because the reflected cylinders are reflected only once, the minus sign is chosen in Eq. (23), as indicated by the minus sign in the arguments above.

$M_{2p}$  can be expressed in as follows

$$\begin{aligned}
 M_{2p;22} &= M_{22} \\
 &= \sum_{n=0}^{\infty} \frac{H_n^2}{2} M_{2(2;R)}(2H_1 + 2n(H_1 + H_2); +) \\
 &\quad + M_{2(2;R)}(2H_2 - 2n(H_1 + H_2); -) \\
 &\quad + \sum_{n=1}^{\infty} \frac{H_n^2}{2} M_{2(2;R)}(2n(H_1 + H_2); +) \\
 &\quad + M_{2(2;R)}(2n(H_1 + H_2); +) \\
 M_{2p;23} &= M_{23}^{(d)} \\
 &= \sum_{n=0}^{\infty} \frac{H_n^2}{2} M_{2(3;R)}(d; 2H_1 + 2n(H_1 + H_2); +) \\
 &\quad + M_{2(3;R)}(d; 2H_2 - 2n(H_1 + H_2); -) \\
 &\quad + \sum_{n=1}^{\infty} \frac{H_n^2}{2} M_{2(3;R)}(d; 2n(H_1 + H_2); +) \\
 &\quad + M_{2(3;R)}(d; 2n(H_1 + H_2); +) :
 \end{aligned} \tag{B 4}$$

Again,  $M_{2p;33}$  is obtained by replacing  $R_1$  by  $R_2$  and  $M_{2p;32} = M_{2p;23}^y$ . Now cylinders can be reflected an arbitrary number of times, thus, for an odd number of reflections the minus sign is chosen in Eq. (23) and for an even number of reflections the plus sign.

#### APPENDIX C: ASYMPTOTIC EXPANSION OF THE FORCE BETWEEN TWO CYLINDERS IN THE PRESENCE OF ONE PLATE

For simplicity, we consider the case of one sidewall and cylinders of equal radius  $R$ . The logarithm of the determinant of the matrix of Eq. (30) with  $n = 1$  can be expressed as

$$\begin{aligned}
 \log \det(M_{1p} M_{1p;l}^{-1}) \\
 &= \sum_{p=1}^{\infty} \frac{1}{p} \text{Tr}(M_{1p;33}^{-1} M_{1p;32} M_{1p;22}^{-1} M_{1p;23})^p \\
 &\quad + d\text{-independent terms;}
 \end{aligned} \tag{C 1}$$

where we have used  $\log \det = \text{Tr} \log$  and expanded the logarithm. Due to the presence of the sidewall, the "self-energy" matrices with elements (see Appendix B)

$$\begin{aligned}
 \lim_{d \rightarrow \infty} M_{1p;22}^{-1} \lim_{d \rightarrow \infty} M_{1p;33}^{-1} \lim_{d \rightarrow \infty} M_{1p;32} \lim_{d \rightarrow \infty} M_{1p;23} \\
 &= \lim_{m \rightarrow 0} I_m^0(Rq) K_m(Rq) - I_m(Rq) I_m^0(Rq) K_{m+m^0}(2Hq)
 \end{aligned} \tag{C 2}$$

for  $D$  modes and

$$\begin{aligned}
 \lim_{d \rightarrow \infty} M_{1p;22}^{-1} \lim_{d \rightarrow \infty} M_{1p;33}^{-1} \lim_{d \rightarrow \infty} M_{1p;32} \lim_{d \rightarrow \infty} M_{1p;23} \\
 &= q^2 [\lim_{m \rightarrow 0} I_m^0(Rq) K_m^0(Rq) + I_m^0(Rq) I_m^0(Rq) K_{m+m^0}(2Hq)]
 \end{aligned} \tag{C 3}$$

for  $N$  modes are non-diagonal. For  $H \ll R$  the non-diagonal part can be treated as a small perturbation, and the matrix can be inverted perturbatively,

$$M_{1p;22}^{-1} = M_{1p;22;l}^{-1} \sum_{n=0}^{\infty} (-1)^n N^n \tag{C 4}$$

where  $M_{1p;22;l}^{-1}$  is the diagonal part of Eqs. (C 2), (C 3) and  $N$  is given by

$$N = \frac{I_m(Rq)}{K_{m^0}(Rq)} K_{m+m^0}(2Hq) \tag{C 5}$$

for  $D$  modes and

$$N = \frac{I_m^0(Rq)}{K_{m^0}^0(Rq)} K_{m+m^0}(2Hq) \tag{C 6}$$

for  $N$  modes. We shall see below that the series of Eq. (C 4) yields a rapidly converging series for the Casimir interaction between the cylinders for all sidewall separations  $H \ll R$ . Since  $d$  is the largest length scale, it is useful to set  $q = u/d$  in Eq. (6) since this allows for expansions of Bessel and Hankel functions that simplify further computations. Using Eq. (C 1), we obtain for the  $d$ -dependent part of the energy the series

$$\begin{aligned}
 E^{D=N} &= \frac{\sim cL}{4 d^2} \sum_{p=1}^{\infty} \frac{1}{p} \text{Tr} \left( M_{1p;33;l}^{-1} \sum_{n=0}^{\infty} (-1)^n N^n \right. \\
 &\quad \left. M_{1p;32} M_{1p;22;l}^{-1} \sum_{n=0}^{\infty} (-1)^n N^n M_{1p;23} \right) :
 \end{aligned} \tag{C 7}$$

To leading order in  $1=d$ , the integral scales as  $1=d^4$ . At this order it is sufficient to consider the term for  $p = 1$  only. Counting the powers of  $1=d$  in the matrix elements appearing in Eq. (C 7) shows that at order  $1=d^4$  it is sufficient to truncate the matrices at order  $m = 1$  for  $D$  modes and  $m = 3$  for  $N$  modes. To leading order in  $1=d$  the matrix elements of  $N$  are  $(R=H)^{m^0+j^0-m^0-j^0}$  and hence independent of  $d$  so that formally all terms of the series over  $n$  have to be included. However, since  $R < H$  the matrix elements of  $N^n$  decrease with increasing  $n$ , yielding a rapidly converging series for the energy. After the expansion in  $1=d$  the integration over  $u$  in Eq. (C 7) can be easily performed for  $N$  modes since the integrand consists of terms that are powers over  $u$  and the Hankel functions  $K_m(u)$ . However, for  $D$  modes, there are logarithmic corrections of the form  $\log(Hu=d)$  and  $1=\log(Ru=2d)$ . For large  $d$ , we can make the approximations  $\log(Hu=d) \approx \log(H=d)$  and  $\log(Ru=2d) \approx \log(R=2d)$  since the main contribution to the integral comes from  $u$  of order unity. With these approximations the integration over  $u$  can be performed analytically. By including terms up to  $n = 5$  in the series of Eq. (C 7), we obtain for the force between

the cylinders from  $N$  modes (with  $r = R=H$ )

$$\begin{aligned} \frac{F_N}{L} = & \frac{148}{5} \frac{R^4}{d^7} \left( 1 + \frac{29}{74} r^2 + \frac{81}{592} r^4 \right. \\ & \left. + \frac{55}{592} r^6 + \frac{625}{9472} r^8 + \frac{201}{4736} r^{10} + \dots + \dots \right) \end{aligned} \quad (C 8)$$

to leading order in  $1=d$ . For  $D$  modes, the general form of the coefficients of the series in  $r$  and its first logarithmic correction can be conjectured from the first few terms. Resummation yields then the closed form expression for the force for all  $r$  to leading order in  $1=d$ ,

$$\begin{aligned} \frac{F_D}{L} = & \frac{\sim c R^4}{d^7} \frac{64}{(4 - r^2)^2} - \frac{64}{\log(R=2d)} \frac{(4 - 3r^2)^2}{r^2 (4 - r^2)^3} \\ & + F_2(r) \log^{-2}(R=2d) + O(\log^{-3}(R=2d)) + \dots \end{aligned} \quad (C 9)$$

Here  $F_2(r) = 4=r^4$  for  $r \rightarrow 0$  so that for  $H = R$  the force is proportional to  $H^4 = (d^7 \log^2(R=2d))$ , which is the same as Eq. (31) up to the different log corrections. Notice that the expansion in  $1=\log(R=2d)$  of Eq. (C 9) is formal and convergence for all  $r$  is not assured in the Dirichlet

case. The reason for that is related to logarithmic corrections  $\log(H=d) = \log(R=2d) + \log(2=r)$  to the matrix elements of  $N$  so that the expansion coefficients grow with  $H$  in a way that higher order coefficients involve higher powers of  $\log(H=d)$ .

The total force is given by the sum  $F_N + F_D$ . From this large distance expansion we can obtain insight into the generation of the non-monotonic behavior of the force. The Neumann force expansion is simple to understand,  $F_N$  decreases in magnitude as the cylinders move away from the plate, i.e.,  $r = R=H$  decreases from 1. Surprisingly, the expansion of the Dirichlet force without the logarithmic terms of Eq. (C 9), i.e. at very large cylinder-cylinder separations  $d$ , indicates that  $F_D$ , similar to  $F_N$ , decreases as the cylinders move away from the plate. But ultimately, as  $H$  increases, the coefficients of the inverse log terms dominate and  $F_D$  increases as the cylinders move away, albeit at a slower rate compared to  $F_N$ , as expected from our numerical results and previous considerations in terms of image charges. If valid, therefore, the expansion not only captures the opposing changes in  $F_D$  and  $F_N$  with sidewall separation but also suggests that  $F_D$  itself has interesting non-monotonic behavior.

- 
- [1] T. Emig, R. L. Jae, M. Kardar, and A. Scardicchio, *Physical Review Letters* 96, 080403 (2006).
  - [2] A. N. Celand and M. L. Roukes, *Appl. Phys. Lett.* 69, 2653 (1996).
  - [3] H. B. Chan, V. A. Aksyuk, R. N. Kleinman, D. J. Bishop, and F. Capasso, *Science* 291, 1941 (2001).
  - [4] V. Sazonova, Y. Yaish, H. Ustunel, D. Roundy, T. A. Arias, and P. L. McEuen, *Nature* 431, 284 (2004).
  - [5] H. B. G. Casimir, *Proc. K. Ned. Akad. Wet.* 51, 793 (1948).
  - [6] M. P. Hertzberg, R. L. Jae, M. Kardar, and A. Scardicchio, *Phys. Rev. Lett.* 95, 250402 (2005).
  - [7] H. B. G. Casimir and D. Polder, *Phys. Rev.* 73, 360 (1948).
  - [8] T. Emig, Fluctuation induced quantum interactions between compact objects and a plane mirror, Preprint arXiv:0712.2199 (2007).
  - [9] A. Scardicchio, *Phys. Rev. D* 72, 065004 (2005), URL <http://link.aps.org/abstract/PRD/v72/p065004>.
  - [10] A. Rodriguez, M. Ibanescu, D. Iannuzzi, F. Capasso, J. D. Joannopoulos, and S. G. Johnson, *Phys. Rev. Lett.* 99, 080401 (2007).
  - [11] S. J. Rahi, A. W. Rodriguez, T. Emig, R. L. Jae, S. G. Johnson, and M. Kardar, *Phys. Rev. A* 77, 030101 (pages 4) (2008), URL <http://link.aps.org/abstract/PRA/v77/e030101>.
  - [12] M. Brown-Hayes, D. A. R. Dalvit, F. D. Mazzitelli, W. J. Kim, and R. Onofrio, *Phys. Rev. A* 72, 052102 (2005).
  - [13] H. Li and M. Kardar, *Phys. Rev. Lett.* 67, 3275 (1991).
  - [14] H. Li and M. Kardar, *Phys. Rev. A* 46, 6490 (1992).
  - [15] R. Buescher and T. Emig, *Physical Review Letters* 94, 133901 (2005).
  - [16] D. A. R. Dalvit, F. C. Lombardo, F. D. Mazzitelli, and R. Onofrio, *Europhys. Lett.* 67, 517 (2004).
  - [17] O. Kenneth, I. Klich, A. Mann, and M. Revzen, *Phys. Rev. Lett.* 89, 033001 (2002).
  - [18] Y. Imry, *Phys. Rev. Lett.* 95, 080404 (2005).
  - [19] J. N. Munday and F. Capasso, *Phys. Rev. A* 75, 060102(R) (2007).
  - [20] U. Leonhardt and T. G. Philbin, *New J. Phys.* 9, 254 (2007).
  - [21] T. Emig, N. Graham, R. L. Jae, and M. Kardar, *Phys. Rev. Lett.* 99, 170403 (2007).
  - [22] T. Emig, N. Graham, R. L. Jae, and M. Kardar, *Phys. Rev. D* 77, 025005 (2008).